We are IntechOpen, the world's leading publisher of Open Access books Built by scientists, for scientists

4,800
Open access books available

122,000
International authors and editors

135M
Downloads

Our authors are among the

154
Countries delivered to

TOP 1%
most cited scientists

12.2%
Contributors from top 500 universities

CLARIVATE ANALYTICS BOOK CITATION INDEX INDEXED

WEB OF SCIENCE™

Selection of our books indexed in the Book Citation Index in Web of Science™ Core Collection (BKCI)

Interested in publishing with us?
Contact book.department@intechopen.com

Numbers displayed above are based on latest data collected.
For more information visit www.intechopen.com

Chapter 11

Electrical Parameter Identification of Single-Phase Induction Motor by RLS Algorithm

Rodrigo Padilha Vieira, Rodrigo Zelir Azzolin, Cristiane Cauduro Gastaldini and Hilton Abílio Gründling

Additional information is available at the end of the chapter

http://dx.doi.org/10.5772/37664

1. Introduction

This chapter addresses the problem of the electrical parameter identification of Single-Phase Induction Motor (SPIM). The knowledge of correct electrical parameters of SPIM allows a better representation of dynamic simulation of this machine. In addition, the identified parameters can improve the performance of the Field Oriented Control (FOC) and sensorless techniques used in these systems.

Controlled induction motor drives have been employed on several appliances in the last decades. Commonly, the control schemes are based on the FOC and sensorless techniques. These methods are mainly applied to three-phase induction machine drives, and a wide number of papers, such as [5, 9, 10, 15, 19, 23, 26] have described such drives. On the other hand, for several years the SPIM has been used in residential appliances, mainly in low power and low cost applications such as in freezers and air conditioning, consuming extensive rate of electrical energy generated in the world. In most of these applications, the SPIM operates at fixed speed and is supplied directly from source grid. However, in the last few years several works have illustrated that the operation with variable speed can enhance the process efficiency achieved by the SPIM ([1, 4, 8, 31]). Furthermore, some other studies have presented high performance drives for SPIM using vector control and sensorless techniques, such as is presented in [7, 12, 18, 24] and [29]. However, these schemes applied on single-phase and three-phase induction motor drives need an accurate knowledge of all electrical parameters machine to have a good performance.

As a consequence of the parameter variation and uncertainties of the machine, literature presents algorithms for computational parameter estimation of induction machines, mainly about three-phase induction machines ([3, 13, 20, 21, 27]). Some authors proposed an on-line

parameter estimation, for adaptive systems and self-tuning controllers due to the fact that the parameters of induction machine change with temperature, saturation, and frequency ([22]).

Differently from the three-phase induction motors, the SPIM is an asymmetrical and coupled machine; these features make the electrical parameter estimation by classical methods difficult, and these characteristics complicate the use of high performance techniques, such as vector and sensorless control. Thus, the use of Recursive Least Square (RLS) algorithm can be a solution for the parameter estimation or self-tuning and adaptive controllers, such as presented in [28] and [30]. Other studies have also been reported in literature describing the parameter estimation of SPIM ([2, 11, 17, 25]).

The aim of this chapter is to provide a methodology to identify a set of parameters for an equivalent SPIM model, and to obtain an improved SPIM representation, as consequence it is possible to design a high performance sensorless SPIM controllers. Here, from the machine model, a classical RLS algorithm is applied at q and d axes based on the current measurements and information of fed voltages with a standstill rotor. The automatized test with standstill rotor can be a good alternative in some applications, such as hermetic compressor systems, where the estimation by conventional methods is a hard task due the fact of the machine is sealed.

An equivalent SPIM behavior representation is obtained with this methodology in comparison with the SPIM model obtained by classical tests. However, some types of SPIM drives, for instance a hermetic system, it is impossible to carried out classical tests. In addition, the proposed methodology has a simple implementation.

This chapter is organized as follows: Section 2 presents the SPIM model, Section 3 gives the RLS parameter algorithm, Section 4 presents and discusses the experimental results obtained with the proposed methodology, and Section 5 gives the main conclusions of this study.

2. Single-phase induction motor model

The commercial SPIM commonly used in low power applications is usually a two-phase induction machine with asymmetrical windings, whose equivalent circuit without the permanent split-capacitor can be represented as in Fig. 1.

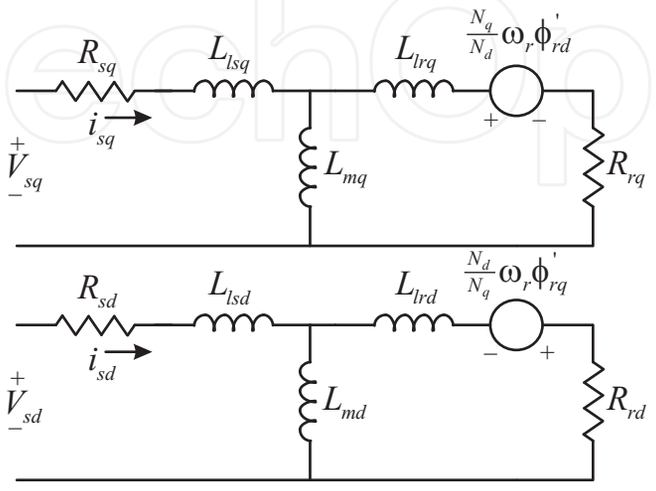

Figure 1. Equivalent circuit of SPIM.

As in [14], in this chapter the squirrel cage SPIM mathematical model is described in a stationary reference-frame by the following equations

$$\begin{bmatrix} V_{sq} \\ V_{sd} \end{bmatrix} = \begin{bmatrix} R_{sq} & 0 \\ 0 & R_{sd} \end{bmatrix} \begin{bmatrix} i_{sq} \\ i_{sd} \end{bmatrix} + \frac{d}{dt} \begin{bmatrix} \phi_{sq} \\ \phi_{sd} \end{bmatrix} \tag{1}$$

$$\begin{bmatrix} V_{rq} \\ V_{rd} \end{bmatrix} = \begin{bmatrix} R_{rq} & 0 \\ 0 & R_{rd} \end{bmatrix} \begin{bmatrix} i_{rq} \\ i_{rd} \end{bmatrix} + \frac{d}{dt} \begin{bmatrix} \phi_{rq} \\ \phi_{rd} \end{bmatrix} + \omega_r \begin{bmatrix} 0 & -1/n \\ n & 0 \end{bmatrix} \begin{bmatrix} \phi_{rq} \\ \phi_{rd} \end{bmatrix} = \begin{bmatrix} 0 \\ 0 \end{bmatrix} \tag{2}$$

$$\begin{bmatrix} \phi_{sq} \\ \phi_{sd} \end{bmatrix} = \begin{bmatrix} L_{sq} & 0 \\ 0 & L_{sd} \end{bmatrix} \begin{bmatrix} i_{sq} \\ i_{sd} \end{bmatrix} + \begin{bmatrix} L_{mq} & 0 \\ 0 & L_{md} \end{bmatrix} \begin{bmatrix} i_{rq} \\ i_{rd} \end{bmatrix} \tag{3}$$

$$\begin{bmatrix} \phi_{rq} \\ \phi_{rd} \end{bmatrix} = \begin{bmatrix} L_{mq} & 0 \\ 0 & L_{md} \end{bmatrix} \begin{bmatrix} i_{sq} \\ i_{sd} \end{bmatrix} + \begin{bmatrix} L_{rq} & 0 \\ 0 & L_{rd} \end{bmatrix} \begin{bmatrix} i_{rq} \\ i_{rd} \end{bmatrix} \tag{4}$$

$$T_e = p(L_{mq} i_{sq} i_{rd} - L_{md} i_{sd} i_{rq}) \tag{5}$$

$$p(T_e - T_L) = J\frac{d\omega_r}{dt} + B_n \omega_r \tag{6}$$

where, the indexes q and d represent the main winding and auxiliary winding, respectively, the indexes sq and sd represent the stator variables, and the indexes rq and rd are used for the rotor variables. V_{sq}, V_{sd}, V_{rq}, V_{rd}, i_{sq}, i_{sd}, i_{rq}, i_{rd}, ϕ_{sq}, ϕ_{sd}, ϕ_{rq}, and ϕ_{rd} are the stator and rotor voltages, currents, and flux; R_{sq}, R_{sd}, R_{rq}, and R_{rd} are the stator and rotor resistances; L_{lsq}, L_{lsd}, L_{lrq}, and L_{lrd} are the leakage inductances; L_{mq} and L_{md} are the mutual inductances; L_{sq}, L_{sd}, L_{rq}, and L_{rd} are the stator and rotor inductances, and are given by: $L_{sq} = L_{lsq} + L_{mq}$, $L_{sd} = L_{lsd} + L_{md}$, $L_{rq} = L_{lrq} + L_{mq}$, and $L_{rd} = L_{lrd} + L_{md}$; N_q and N_d represent the number of turns for the main and auxiliary windings, respectively; p is the pole pair number and ω_r is the rotor speed, and n is the relationship between the number of turns for auxiliary and for main winding N_d/N_q. T_e is the electromagnetic torque, T_L is the load torque, B_n is the viscous friction coefficient, and J is the inertia coefficient.

From (1) - (4) it is possible to obtain the differential equations that express the dynamical behavior of the SPIM, as follows,

$$\frac{d}{dt} i_{sq} = -\frac{R_{sq} L_{rq}}{\overline{\sigma}_q} i_{sq} - \omega_r \frac{1}{n} \frac{L_{mq} L_{md}}{\overline{\sigma}_q} i_{sd} + \frac{R_{rq} L_{mq}}{\overline{\sigma}_q} i_{rq} - \omega_r \frac{1}{n} \frac{L_{rd} L_{mq}}{\overline{\sigma}_q} i_{rd} + \frac{L_{rq}}{\overline{\sigma}_q} V_{sq} \tag{7}$$

$$\frac{d}{dt} i_{sd} = \omega_r n \frac{L_{md} L_{mq}}{\overline{\sigma}_d} i_{sq} - \frac{L_{rd} R_{sd}}{\overline{\sigma}_d} i_{sd} + \omega_r n \frac{L_{rq} L_{md}}{\overline{\sigma}_d} i_{rq} + \frac{R_{rd} L_{md}}{\overline{\sigma}_d} i_{rd} + \frac{L_{rd}}{\overline{\sigma}_d} V_{sd} \tag{8}$$

$$\frac{d}{dt} i_{rq} = \frac{L_{mq} R_{sq}}{\overline{\sigma}_q} i_{sq} + \omega_r \frac{1}{n} \frac{L_{sq} L_{md}}{\overline{\sigma}_q} i_{sd} - \frac{L_{sq} R_{rq}}{\overline{\sigma}_q} i_{rq} + \omega_r \frac{1}{n} \frac{L_{sq} L_{rd}}{\overline{\sigma}_q} i_{rd} - \frac{L_{mq}}{\overline{\sigma}_q} V_{sq} \tag{9}$$

$$\frac{d}{dt} i_{rd} = -\omega_r n \frac{L_{sd} L_{mq}}{\overline{\sigma}_d} i_{sq} + \frac{L_{md} R_{sd}}{\overline{\sigma}_d} i_{sd} - \omega_r n \frac{L_{sd} L_{rq}}{\overline{\sigma}_d} i_{rq} - \frac{L_{sd} R_{rd}}{\overline{\sigma}_d} i_{rd} - \frac{L_{md}}{\overline{\sigma}_d} V_{sd} \tag{10}$$

where $\overline{\sigma}_q = L_{sq}L_{rq} - L_{mq}^2$, $\overline{\sigma}_d = L_{sd}L_{rd} - L_{md}^2$.

The transfer functions in the axes q and d at a standstill rotor ($\omega_r = 0$) are obtained from (7)-(10), where these functions are decoupled and presented in (11) and (12).

$$H_q(s) = \frac{i_{sq}(s)}{V_{sq}(s)} = \frac{s\overline{\sigma}_q^{-1}L_{rq} + \overline{\sigma}_q^{-1}\tau_{rq}^{-1}L_{rq}}{s^2 + sp_q + \overline{\sigma}_q^{-1}R_{rq}R_{sq}} \tag{11}$$

$$H_d(s) = \frac{i_{sd}(s)}{V_{sd}(s)} = \frac{s\overline{\sigma}_d^{-1}L_{rd} + \overline{\sigma}_d^{-1}\tau_{rd}^{-1}L_{rd}}{s^2 + sp_d + \overline{\sigma}_d^{-1}R_{rd}R_{sd}} \tag{12}$$

where $p_q = \left(R_{sq}L_{rq} + R_{rq}L_{sq}\right)/\overline{\sigma}_q$ and $p_d = \left(R_{sd}L_{rd} + R_{rd}L_{sd}\right)/\overline{\sigma}_d$.

3. Parameter identification of single-phase induction machine

In section 2, the decoupled transfer functions of the SPIM were obtained assuming a standstill rotor ($\omega_r = 0$). Thus, in this section the parameter identification is achieved with SPIM at a standstill rotor by a RLS algorithm. The identification with a standstill rotor is appropriated in some cases such as hermetic refrigeration compressors ([28]). The RLS identification algorithm requires the plant model in a discrete time linear regression form. Assuming the actual sampling index k, the regression model is given by

$$\hat{\mathbf{Y}}(k) = \phi^T(k)\theta(k) \tag{13}$$

The recursive algorithm is achieved with the equations (14)-(17).

$$e(k) = \mathbf{Y}(k) - \hat{\mathbf{Y}}(k) \tag{14}$$

$$\mathbf{K}(k) = \frac{\mathbf{P}(k-1)\phi(k)}{1 + \phi^T(k)\mathbf{P}(k-1)\phi(k)} \tag{15}$$

$$\theta(k) = \theta(k-1) + \mathbf{K}(k)e(k) \tag{16}$$

$$\mathbf{P}(k) = \left(I - \mathbf{K}(k)\phi^T(k)\right)\mathbf{P}(k-1) \tag{17}$$

where $dim\ \mathbf{Y} = \bar{M} \times \bar{N}$, $dim\ \phi^T(k) = \bar{M} \times \bar{r}$

$dim\ \theta(k) = \bar{r} \times \bar{N}$, $dim\ e(k) = \bar{M} \times \bar{N}$

$dim\ \mathbf{K}(k) = \bar{r} \times \bar{M}$, $dim\ I = dim\ \mathbf{P}(k) = \bar{r} \times \bar{r}$

From the equations (11) and (12) it is possible to reformulate the estimation parameter problem based on a linear regression model. Here, the parameter estimation method is divided into two steps:

***First step**: estimation of (18) and (19) vide equations (20) and (21) :*

This step consists into obtaining a linear-time-invariant model of the SPIM. The identification of b_1, b_0, a_1 and a_0 is done by performing a standstill test. The coefficients presented in (11) and (12) are functions of the machine parameters. For simplicity, the transfer functions given in (11) and (12) are rewritten in two transfer functions given by (18) and (19).

$$H_q(s) = \frac{i_{sq}^s(s)}{V_{sq}^s(s)} = \frac{sb_{1q} + b_{0q}}{s^2 + sa_{1q} + a_{0q}} \tag{18}$$

and

$$H_d(s) = \frac{i^s_{sd}(s)}{V^s_{sd}(s)} = \frac{sb_{1d} + b_{0d}}{s^2 + sa_{1d} + a_{0d}} \tag{19}$$

where

$$b_{1q} = \frac{L_{rq}}{\overline{\sigma}_q}, b_{0q} = \frac{L_{rq}}{\overline{\sigma}_q \tau_{rq}}, \quad a_{1q} = \frac{R_{sq}L_{rq} + R_{rq}L_{sq}}{\overline{\sigma}_q}, a_{0q} = \frac{R_{sq}R_{rq}}{\overline{\sigma}_q} \tag{20}$$

and

$$b_{1d} = \frac{L_{rd}}{\overline{\sigma}_d}, b_{0d} = \frac{L_{rd}}{\overline{\sigma}_d \tau_{rd}}, \quad a_{1d} = \frac{R_{sd}L_{rd} + R_{rd}L_{sd}}{\overline{\sigma}_d}, a_{0d} = \frac{R_{sd}R_{rd}}{\overline{\sigma}_d} \tag{21}$$

In order to obtain the regression linear model the transfer functions of (18) and (19) can be generalized and rewritten as,

$$\frac{d^2 i_{sq}}{dt^2} + a_{1q}\frac{di_{sq}}{dt} + a_{0q} i_{sq} = b_{1q}\frac{dV_{sq}}{dt} + b_{0q} V_{sq} \tag{22}$$

and

$$\frac{d^2 i_{sd}}{dt^2} + a_{1d}\frac{di_{sd}}{dt} + a_{0d} i_{sd} = b_{1d}\frac{dV_{sd}}{dt} + b_{0d} V_{sd} \tag{23}$$

Solving for the second derivative of the stator current,

$$\frac{d^2 i_{sq}}{dt^2} = \begin{bmatrix} -\frac{di_{sq}}{dt} & -i_{sq} & \frac{dV_{sq}}{dt} & V_{sq} \end{bmatrix} \begin{bmatrix} a_{1q} \\ a_{0q} \\ b_{1q} \\ b_{0q} \end{bmatrix} \tag{24}$$

and

$$\frac{d^2 i_{sd}}{dt^2} = \begin{bmatrix} -\frac{di_{sd}}{dt} & -i_{sd} & \frac{dV_{sd}}{dt} & V_{sd} \end{bmatrix} \begin{bmatrix} a_{1d} \\ a_{0d} \\ b_{1d} \\ b_{0d} \end{bmatrix} \tag{25}$$

The estimation of coefficients b_{1q}, b_{0q}, a_{1q}, a_{0q}, b_{1d}, b_{0d}, a_{1d} and a_{0d} is done by using RLS estimation algorithm described in the equations (13)-(17). The linear regression model form (13) is given for the q axis by the following equations,

$$\mathbf{Y}_q(k) = \frac{d^2 i_{sq}}{dt^2} \tag{26}$$

$$\phi_q^T(k) = \begin{bmatrix} -\frac{di_{sq}}{dt} & -i_{sq} & \frac{dV_{sq}}{dt} & V_{sq} \end{bmatrix} \tag{27}$$

$$\theta_q^T(k) = \begin{bmatrix} a_{1q} & a_{0q} & b_{1q} & b_{0q} \end{bmatrix} \tag{28}$$

And, for the d axis,

$$\mathbf{Y}_d(k) = \frac{d^2 i_{sd}}{dt^2} \tag{29}$$

$$\phi_d^T(k) = \begin{bmatrix} -\frac{di_{sd}}{dt} & -i_{sd} & \frac{dV_{sd}}{dt} & V_{sd} \end{bmatrix} \tag{30}$$

$$\theta_d^T(k) = \begin{bmatrix} a_{1d} & a_{0d} & b_{1d} & b_{0d} \end{bmatrix} \tag{31}$$

where, let us assume that the derivatives presented in (26)-(27) and (29)-(30) are measurable quantities. In the implementation, these quantities are obtained by State Variable Filters (SVF) such as in [6]. Four SVF filters were developed by discretization of the continuous-time transfer function given by,

$$\frac{V_{sqf}}{V_{sq}} = \frac{V_{sdf}}{V_{sd}} = \frac{i_{sqf}}{i_{sq}} = \frac{i_{sdf}}{i_{sd}} = G_{svf}(s) = \frac{\omega_{svf}^3}{(s+\omega_{svf})^3} \tag{32}$$

where, ω_{svf} is the filter bandwidth defined at around 5 to 10 times the input frequency signal. Here, $\omega_{svf} = \omega$, and ω is signal frequency, and the signals V_{sq}, V_{sd}, i_{sq}, and i_{sd} are used to obtain the filtered signals V_{sqf}, V_{sdf}, i_{sqf} and i_{sdf}.

The discretized transfer function, using the Euler method and sampling time of T_s, can be performed in state-space as

$$\mathbf{x}_{svf(k+1)} = \left(1 + \mathbf{A}_{svf}T_s\right)\mathbf{x}_{svf(k)} + T_s\mathbf{B}_{svf}u_{svf(k)} \tag{33}$$

where, $\mathbf{A}_{svf} = \begin{bmatrix} 0 & 1 & 0 \\ 0 & 0 & 1 \\ -\omega_{svf}^3 & -3\omega_{svf}^2 & 3\omega_{svf} \end{bmatrix}$, $\mathbf{B}_{svf} = \begin{bmatrix} 0 \\ 0 \\ \omega_{svf}^3 \end{bmatrix}$, $x_{svf} = \begin{bmatrix} x_1 \\ x_2 \\ x_3 \end{bmatrix}$ The variable u_{svf} represents the input signal, while the state variables x_1, x_2 and x_3 represent the input filtered signal, first derivative signal and second derivative signal, respectively.

With the SVF it is possible to avoid the use o low-pass filters in signals of the currents and the voltages, due the fact of the SVF has behavior of a low-pass filter. In addition, due this characteristic the SVF atenues the impact of pulsed and noise signals on the measurements of stator currents. For instance, to demonstrate the response of SVF Figure 2 presents the Module and the Phase Bode diagram with bandwidth of $\omega_{svf} = 5 * 2\pi * 30Hz\ [rad/s]$. It is possible to observer that the high frequency signals are attenuated.

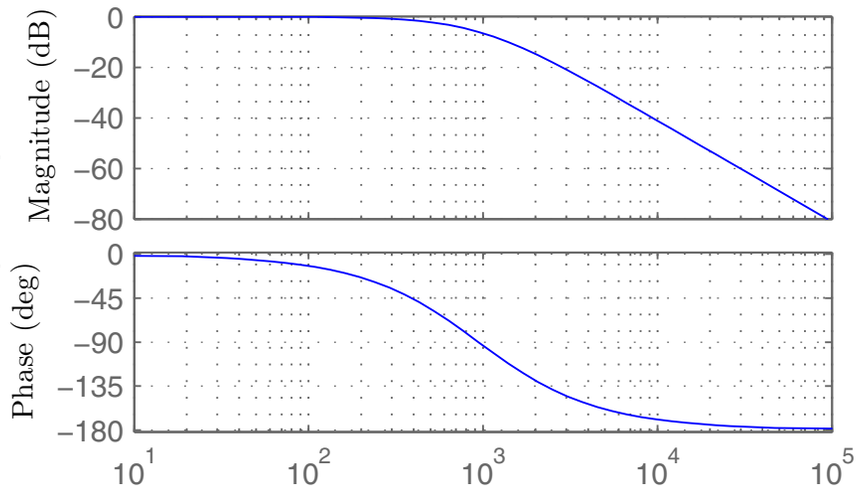

Figure 2. Bode diagram of the State Variable Filter.

***Second step**: identification of machine parameters, R_{sq}, R_{sd}, R_{rq}, R_{rd}, L_{mq}, L_{md}, L_{sq}, L_{sd}, L_{rq} and, L_{rd}:*

The electrical parameters of the SPIM are obtained combining the identified coefficients of $\theta_q(k)$ and $\theta_d(k)$ in (28) and (31) with the coefficients of the transfer functions (20) and (21), respectively, after the convergence of the RLS algorithm by the equations (34) and (35). In the numerical solution, the stator and rotor inductances are considered to have the same values in each winding.

$$\begin{aligned}
\hat{R}_{sq} &= \frac{a_{0q}}{b_{0q}} \\
\hat{R}_{rq} &= \frac{a_{1q}}{b_{1q}} - \hat{R}_{sq} \\
\hat{L}_{mq} &= \frac{\sqrt{\hat{R}_{rq}\left(b_{1q}^2\hat{R}_{rq} - b_{0q}\right)}}{b_{0q}} \\
\hat{L}_{sq} &= \hat{L}_{rq} = \hat{R}_{rq}\frac{b_{1q}}{b_{0q}}
\end{aligned} \tag{34}$$

$$\begin{aligned}
\hat{R}_{sd} &= \frac{a_{0d}}{b_{0d}} \\
\hat{R}_{rd} &= \frac{a_{1d}}{b_{1d}} - \hat{R}_{sd} \\
\hat{L}_{md} &= \frac{\sqrt{\hat{R}_{rd}\left(b_{1d}^2\hat{R}_{rd} - b_{0d}\right)}}{b_{0d}} \\
\hat{L}_{sd} &= \hat{L}_{rd} = \hat{R}_{rd}\frac{b_{1d}}{b_{0d}}
\end{aligned} \tag{35}$$

4. Results and discussions

The RLS parameter identification algorithm presented in this chapter is implemented in a DSP based platform using TMS320F2812 DSP and a three-leg voltage source inverter. Figure 3 shows the diagram of the system to obtain the experimental results. The machine used for the validation of this methodology is a SPIM of a commercial hermetic refrigeration compressor of an air conditioning. The SPIM was removed from the hermetic compressor to achieve classical tests. The machine is two-pole, 220 V type. In the implementation of RLS identification parameter algorithm, the DC bus was limited in 177V/5A, and the sampling time of $400\mu s$ was used.

As described in Sections 2 and 3, the experiment for the parameter identification is achieved with a standstill rotor. In the first step, a square wave with variable frequency and reduced voltage supplies the main winding, while the auxiliary winding is opened. The stator current in the main winding is measured using hall effect sensor. The voltage used in this algorithm is estimated by the product of modulation and DC bus indexes. After the identification for the main winding, the same procedure is repeated for the auxiliary winding. The square wave is used for better excitation of the plant.

The frequency of the supply voltage is 5 Hz in the estimation of resistances to minimize the skin effect, and it is 30 Hz for the estimation of inductances.

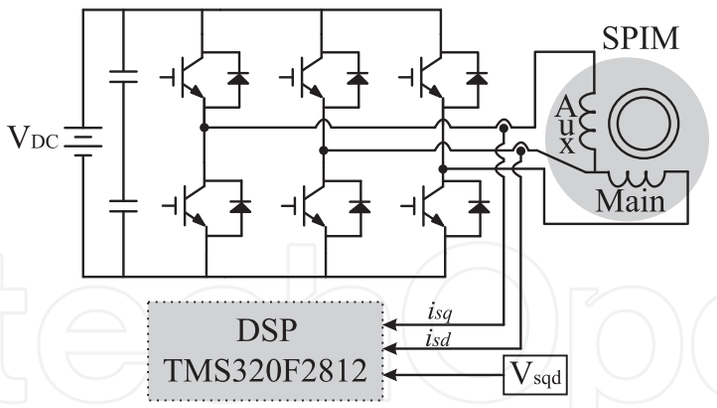

Figure 3. System diagram for the experimental results.

The first test for the identification of stator and rotor resistances is achieved in the main winding. The convergence of coefficients θ_q for this winding is presented in Fig. 4. Fig. 4 (a) presents the coefficients a_{1q} and a_{0q}, while Fig. 4 (b) gives the coefficients b_{1q} and b_{0q}. In this experiment the frequency of the supply voltage is selected on 5 Hz. As presented in figures, the coefficient convergence is fast and it is excited by the reset of the covariance matrix (**P**). Here, the reset of the covariance matrix (**P**) is used to avoid that this matrix reach zero and consequently loses the ability of to update the parameter matrix ($\theta_q(k)$). Some oscillations are introduced every time that the covariance matrix (**P**) is reset, but the convergence of coefficients $\theta_q(k)$ is stable around a region.

The aim of the algorithm (13)-(17) is to identify a set of parameters that produce a good dynamic response such as real dynamic response of the induction machine. If it is necessary to ensure the parameter convergence to the true values the Lemma 12.5.2 (Persistent Excitation) of [16] must be satisfied. However, in practical implementations the designer normally unknown the exactly parameter values due the assumptions and approximations made to develop the mathematical model of the plant, and due the presence of unmodulated dynamics in the system, such as the measurement and drive systems.

The coefficients used in the electrical parameter calculation are the final values of Fig 4. The coefficient convergence for d axis has behavior similar to coefficient convergence for q axis in Fig. 4.

Table 1 shows the final obtained coefficients a_{1q}, a_{0q}, b_{1q}, and b_{0q} in a q axis when the voltage frequency is 5 Hz and 30 Hz. Table 2 shows the final obtained coefficients a_{1d}, a_{0d}, b_{1d}, and b_{0d} in a d axis when the voltage frequency is 5 Hz and 30 Hz. From Fig. 4 it can be observed that the coefficient convergence is fast.

	5 Hz	30 Hz
a_{1q}	244.27	707.64
a_{0q}	447.96	8084.14
b_{1q}	24.82	27.73
b_{0q}	128.58	2913.7

Table 1. Final convergence for coefficients of the main winding.

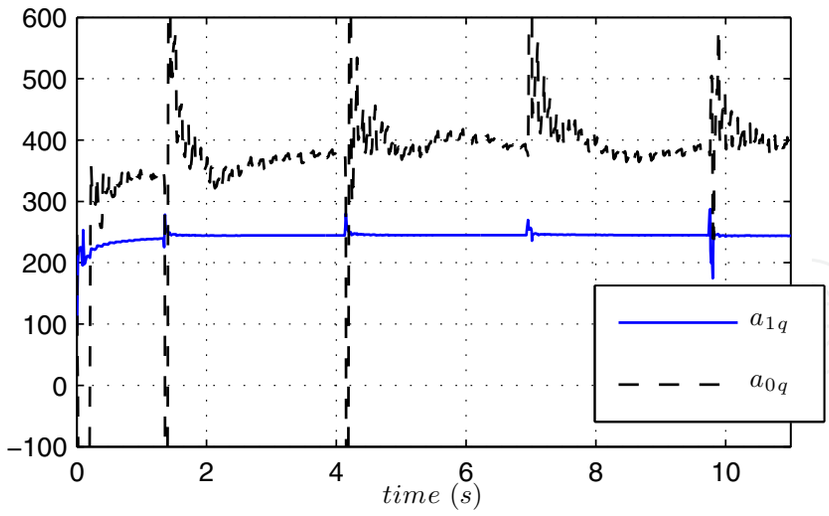

(a)

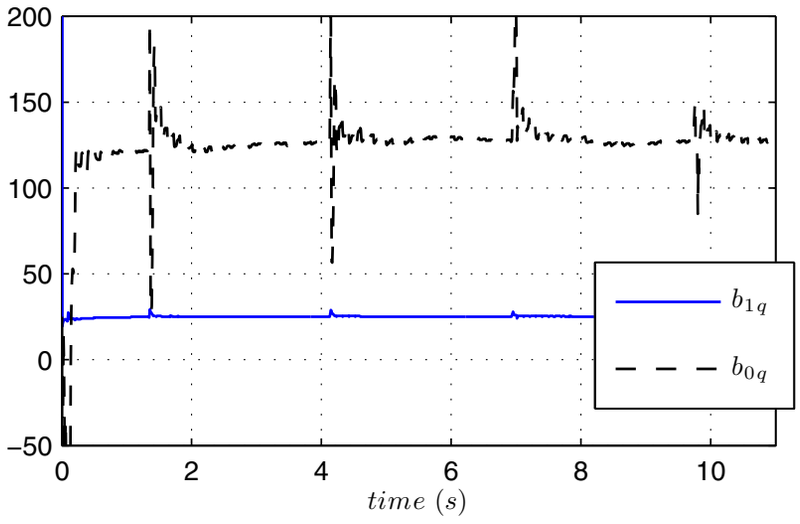

(b)

Figure 4. Coefficients convergence.

	5 Hz	30 Hz
a_{1d}	246.15	779.65
a_{0d}	559.4	3304.5
b_{1d}	9.83	17.62
b_{0d}	43.67	2448.17

Table 2. Final convergence for coefficients of the auxiliary winding.

The electrical parameters of the induction machine are obtained combining the final value of coefficients in Table 1 and Table 2 with the equations (34) and (35), respectively. Table 3 presents the identified electrical parameters of SPIM. In this study we also make a comparison with the results obtained by classical methods, thus, the SPIM identified by RLS algorithm is

also tested using no-load and standstill classical methods. The electrical parameters estimated when the SPIM is tested by classical methods are shown in Table 4.

	R_{sq}	R_{rq}	L_{mq}	$L_{sq} = L_{rq}$
Identified	3.62Ω	6.27Ω	0.2186H	0.2376H
	R_{sd}	R_{rd}	L_{md}	$L_{sd} = L_{rd}$
Identified	12.79Ω	12.23Ω	0.2849H	0.3142H

Table 3. Experimental identified electrical parameters by RLS algorithm.

	R_{sq}	R_{rq}	L_{mq}	$L_{sq} = L_{rq}$
Estimated	3.95Ω	5.1506Ω	0.2149H	0.2292H
	R_{sd}	R_{rd}	L_{md}	$L_{sd} = L_{rd}$
Estimated	11.95Ω	8.6463Ω	0.382H	0.401H

Table 4. Electrical parameters estimated by classical tests.

Aiming the model validation, two experiments are carried out. In the first experiment, the SPIM is driven by a *v/f* strategy at no-load operation, thus, the main and the auxiliary windings are supplied by controlled voltages varying the frequency from zero until a steady-state condition. The rotor speed and the stator currents are also measured. These measurements are recorded for posterior comparison with simulated values.

The model of single-phase induction machine presented in equations (7)-(10) is simulated using the estimated parameters of the machine by RLS algorithm given in Table 3. The model is also simulated using the parameters estimated by the classical methods presented in Table 4. The simulated stator currents are compared with the measured stator currents. The induction motor model equations (7)-(10) are discretized using the Euler Method in the same frequency of the experimental commutation for this test at 5 kHz. The recorded rotor speed is used in the simulated model to make it independent of the mechanical parameters.

In the first experimental result, the frequency of stator voltages varies from zero until 25 Hz and it is fixed in 25 Hz, by the *v/f* method. The recorded voltage values are used to supply the SPIM model in the simulation. Thus, from the same input voltages, Fig. 5 shows currents simulated and measured for the main winding in the first experiment. Fig. 5 (a) presents the comparison between the simulation of i_{sq} current with parameters estimated by RLS algorithm, and the experimental measurement of i_{sq} current, and Fig 5 (b) presents the comparison of the i_{sq} current when the simulations is carried out with parameters estimated by classical tests.

Fig. 6 presents a detail of the comparison between the measured and the simulated currents in steady-state condition for the main winding. In Fig. 6 (a) the comparison between experimental current and simulated current is presented when the SPIM parameters are estimated by RLS algorithm, while Fig. 6 (b) presents the comparison between experimental current and simulated current when the SPIM parameters are estimated by classical tests.

Fig. 7 presents a comparison among i_{sd} currents on the first experiment. Fig. 7 (a) shows the simulated current using parameters estimated by RLS algorithm in the SPIM model and the

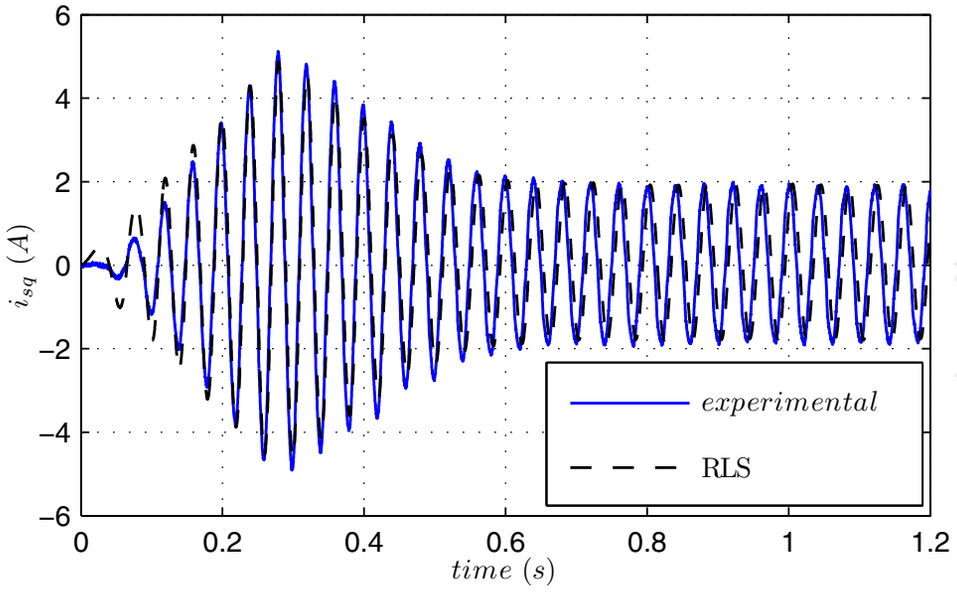

(a)

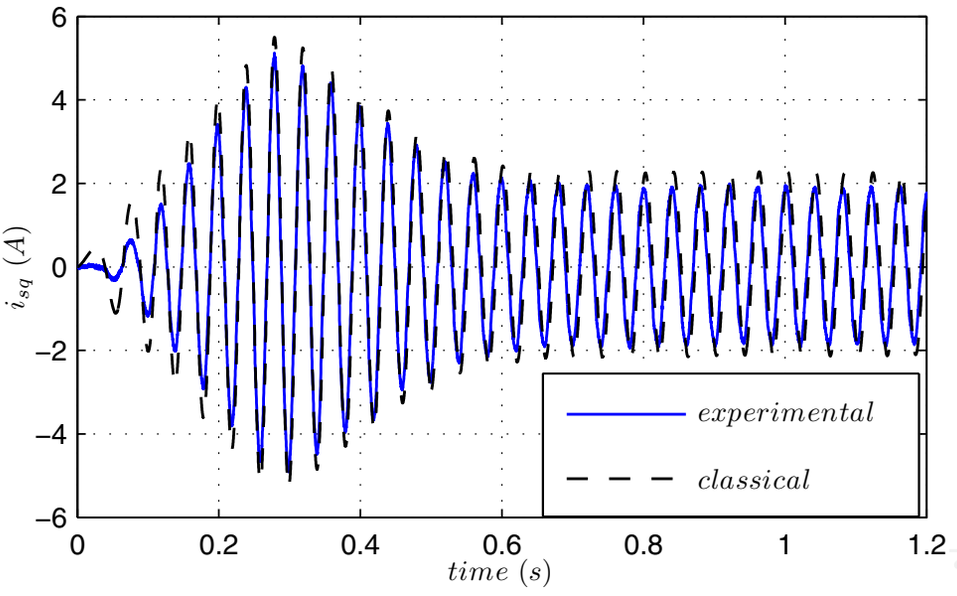

(b)

Figure 5. Comparison among measured and simulated currents for the first test. (a) Simulated i_{sq} using parameters estimated with RLS algorithm and measured i_{sq} current. (b) Simulated i_{sq} current using parameters estimated by classical tests and measured i_{sq} current.

measured i_{sd} current. Fig. 7 (b) gives the simulated current using parameters estimated by classical tests and the measured current.

Fig. 8 shows the comparison between i_{sd} currents in steady-state condition, Fig. 8 (a) gives the comparison between the measured i_{sd} current and the simulated i_{sd} current using SPIM parameters estimated by the RLS algorithm, whereas, Fig. 8 (b) presents the comparison

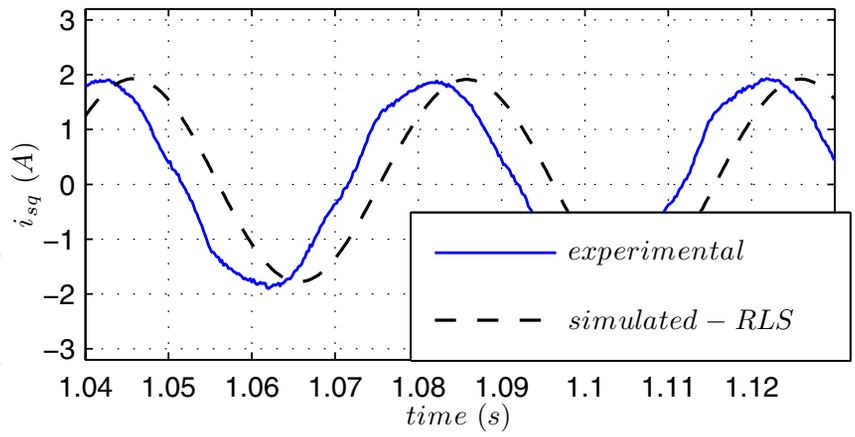

(a)

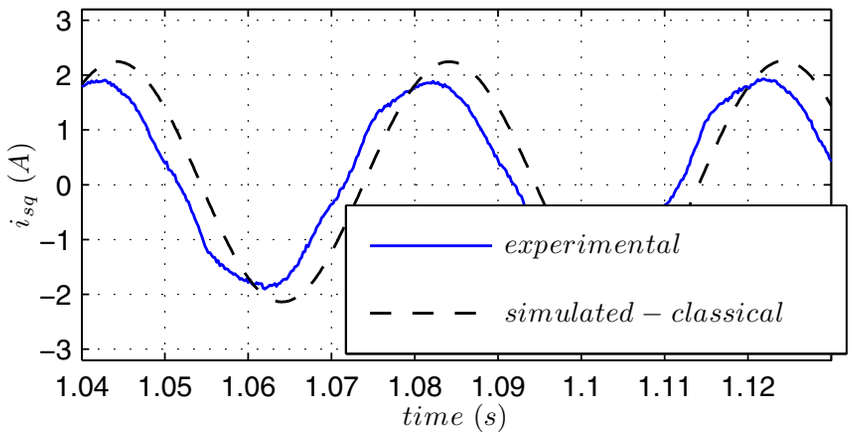

(b)

Figure 6. Comparison between measured and simulated currents at 25 Hz. (a) Simulated (RLS - Parameters) and measured i_{sq} currents. (b) Simulated (Classical - Parameters) and measured i_{sq} currents.

between the measured i_{sd} current and the simulated i_{sd} current using classical method for parameter estimation.

From Figures 5-8 it is possible to observer the good matching between the simulated and experimental currents for the q and d axes. In addition, some small discrepancies are found in these figures due the parameter inaccuracies and unmodulated effects (for instance the measurement and drive systems).

The advantage of the methodology presented in this chapter employing the RLS algorithm is that some types of applications, such as hermetic compressor, it is impossible carried out classical tests for estimation of the electrical parameters of the SPIM. In addition, the methodology has simplicity in implementation.

In the second experiment, the frequency of the supplied voltages of SPIM varies from zero until 30 Hz, and it is fixed at 30 Hz. As in the previous test, this is a no-load test and the SPIM is driven by a *v/f* strategy. The stator currents and rotor speed are measured and recorded.

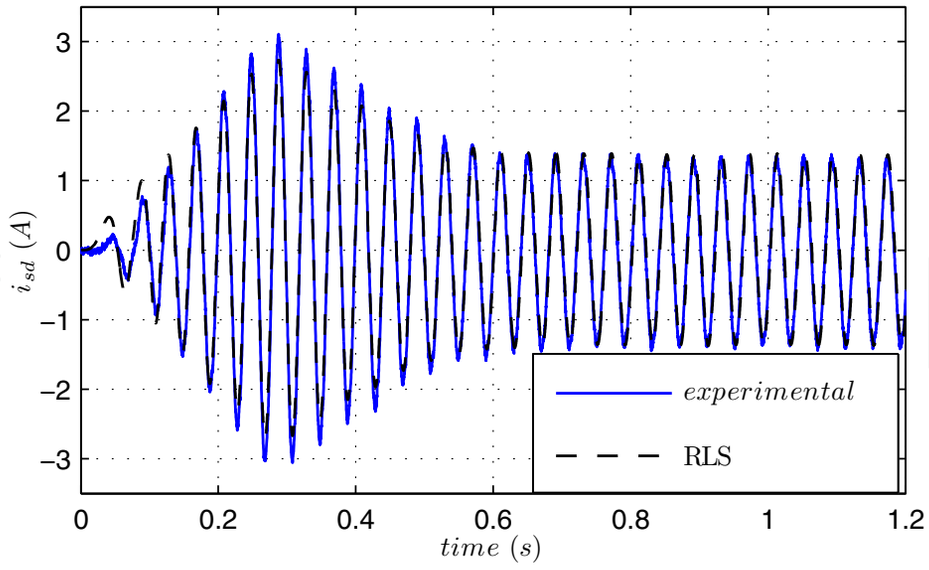

(a)

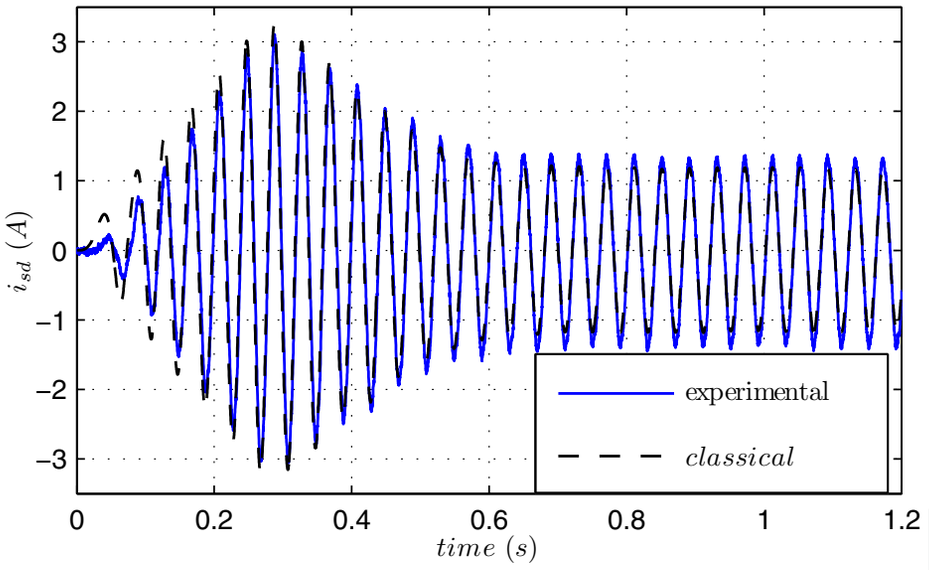

(b)

Figure 7. Comparison among i_{sd} currents in first test. (a) Simulated i_{sd} current by RLS parameter estimation and measured i_{sd} current. (b) Simulated i_{sd} current by classical tests and measured i_{sd} current.

Fig. 9 presents a comparison between measured and simulated i_{sq} currents in steady-stead condition. In Fig. 9 (a) shows the measured i_{sq} current and the simulated i_{sq} current using parameters estimated by RLS algorithm on the SPIM model, while Fig. 9 (b) gives the measured i_{sq} and the simulated i_{sq} current using parameters estimated by classical tests.

Fig. 10 presents a comparison between i_{sd} currents in steady-state condition for the second test.

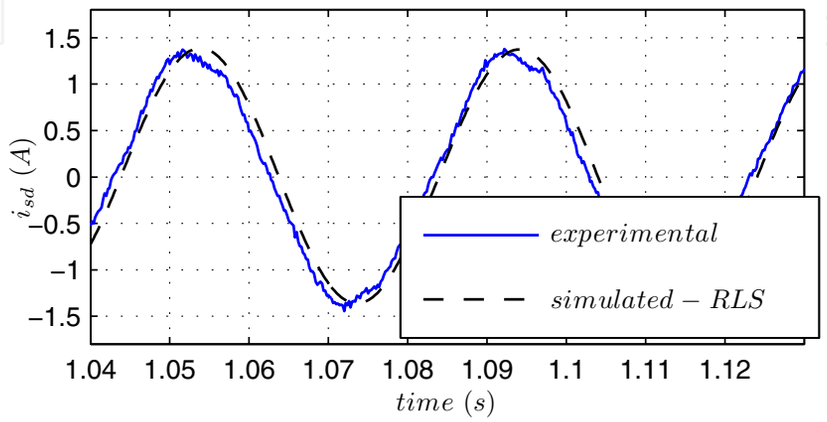

(a)

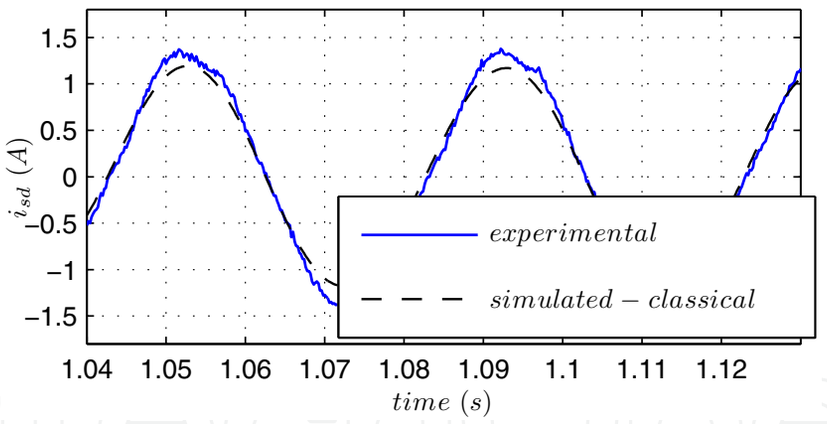

(b)

Figure 8. Comparison between i_{sd} currents at 25 Hz. (a) Simulated (RLS - parameter) and measured i_{sd} currents. (b) Simulated (classical tests) and measured i_{sd} currents.

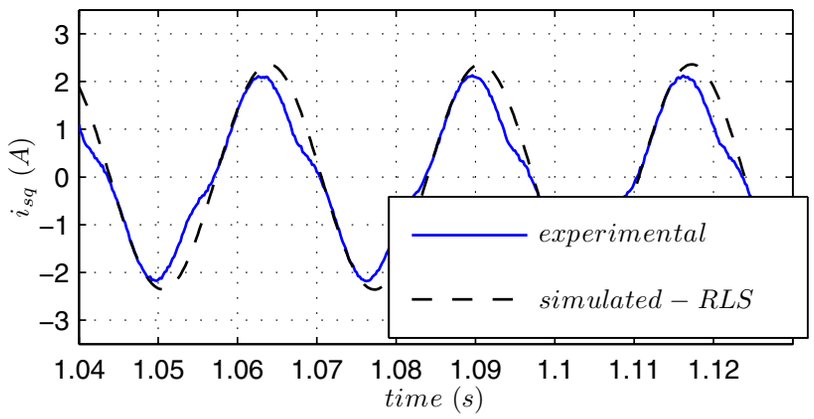

(a)

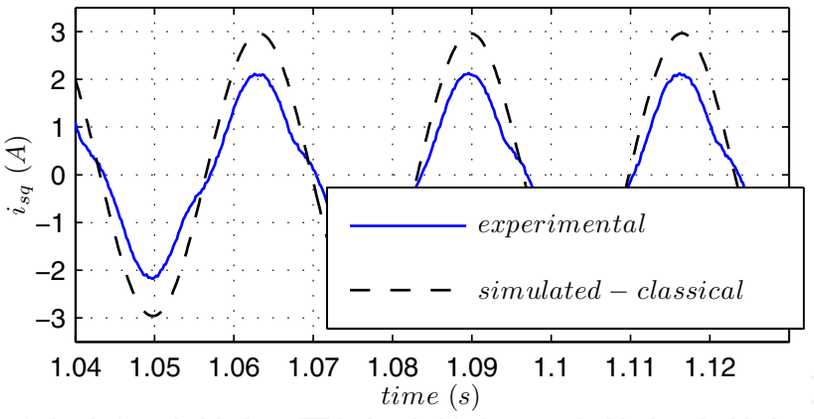

(b)

Figure 9. Comparison between i_{sq} currents at 30 Hz in steady-state condition. (a) Simulated (RLS - parameter) and measured i_{sq} currents. (b) Simulated (classical tests) and measured i_{sq} currents.

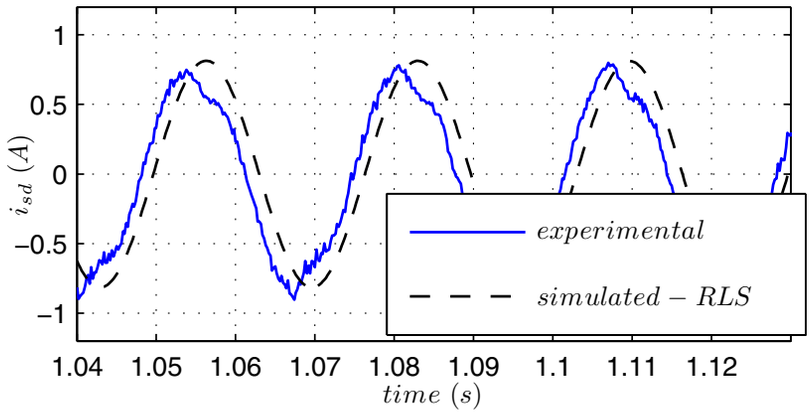

(a)

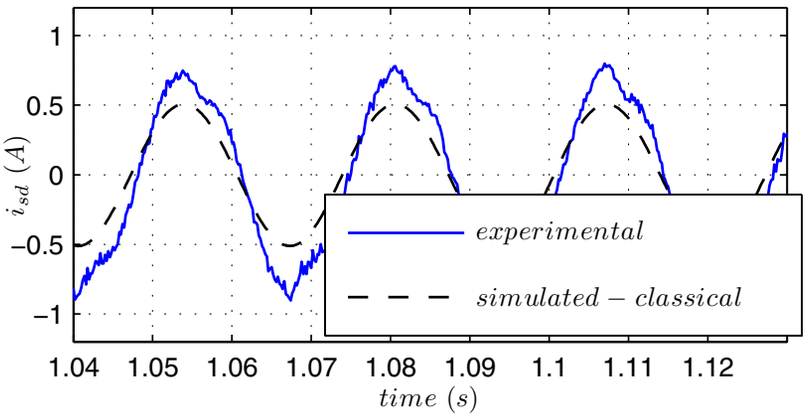

(b)

Figure 10. Comparison between i_{sd} currents at 30 Hz. (a) Simulated (RLS - parameter) and measured i_{sd} currents. (b) Simulated (classical tests) and measured i_{sd} currents.

5. Conclusion

A methodology for single-phase induction machine parameter identification was presented and discussed in this chapter. The machine tested was a SPIM used in a hermetic compressor of air conditioning. Using the proposed methodology it is possible to obtain all electrical parameters of SPIM for simulation and design of high performance vector control and sensorless SPIM drives. The main contribution of this study is the development of an automatized procedure for the identification of all electrical parameters of SPIM, such as the SPIM used in hermetic conditioning compressor. Experimental results demonstrate the effectiveness of the method. Some experimental comparisons among measurements and simulations using parameters estimated by classical tests and simulations using parameters obtained by RLS algorithm are presented. From Table 3 and Table 4 it is possible to observe that the parameters obtained with RLS algorithm converge to different values compared to classical tests. However, the results in Fig. 5 - 10 show that the parameters estimated with RLS algorithm present equivalent dynamical behavior compared with parameters estimated by classical methods. The methodology proposed in this chapter can be extended to be applied in other SPIM drives and three-phase induction motor drives.

Author details

Rodrigo Padilha Vieira
Federal University of Pampa - UNIPAMPA, Federal University of Santa Maria - UFSM, Power Electronics and Control Research Group - GEPOC, Brazil

Rodrigo Zelir Azzolin
Federal University of Rio Grande - FURG, Federal University of Santa Maria - UFSM, Power Electronics and Control Research Group - GEPOC, Brazil

Cristiane Cauduro Gastaldini
Federal University of Pampa - UNIPAMPA, Federal University of Santa Maria - UFSM, Power Electronics and Control Research Group - GEPOC, Brazil

Hilton Abílio Gründling
Federal University of Santa Maria - UFSM, Power Electronics and Control Research Group - GEPOC, Brazil

6. References

[1] Amin, A., El Korfally, M., Sayed, A. & Hegazy, O. [2009]. Efficiency optimization of two-asymmetrical-winding induction motor based on swarm intelligence, *IEEE Transactions on Energy Conversion* 24(1): 12 –20.

[2] Azzolin, R. Z., Gastaldini, C. C., Vieira, R. P. & Gründling, H. A. [2011]. *A RMRAC Parameter Identification Algorithm Applied to Induction Machines, Electric Machines and Drives, Miroslav Chomat (Ed.)*, InTech.

[3] Azzolin, R. Z. & Gründling, H. A. [2009]. A MRAC parameter identification algorithm for three-phase induction motors, *IEEE International Electric Machines and Drives Conference, IEMDC '09.*, pp. 273 –278.

[4] Blaabjerg, F., Lungeanu, F., Skaug, K. & Tonnes, M. [2004]. Two-phase induction motor drives, *IEEE Industry Applications Magazine* 10(4): 24–32.

[5] Bose, B. [2009]. Power electronics and motor drives recent progress and perspective, *IEEE Transactions on Industrial Electronics* 56(2): 581 –588.

[6] Câmara, H. T., Cardoso, R. C., Azzolin, R. Z., Pinheiro, H. & Gründling, H. A. [2006]. Low-cost sensorless induction motor speed control, *IEEE 32nd Annual Conference on Industrial Electronics, IECON 2006*, pp. 1200 –1205.

[7] de Rossiter Corrêa, M., Jacobina, C., Lima, A. & da Silva, E. [2000]. Rotor-flux-oriented control of a single-phase induction motor drive, *IEEE Transactions on Industrial Electronics* 47(4): 832–841.

[8] Donlon, J., Achhammer, J., Iwamoto, H. & Iwasaki, M. [2002]. Power modules for appliance motor control, *IEEE Industry Applications Magazine* 8(4): 26–34.

[9] Finch, J. & Giaouris, D. [2008]. Controlled AC electrical drives, *IEEE Transactions on Industrial Electronics* 55(2): 481 –491.

[10] Holtz, J. [2005]. Sensorless control of induction machines: With or without signal injection?, *IEEE Transactions on Industrial Electronics* 53(1): 7 – 30.

[11] Hrabovcova, V., Kalamen, L., Sekerak, P. & Rafajdus, P. [2010]. Determination of single phase induction motor parameters, *International Symposium on Power Electronics Electrical Drives Automation and Motion (SPEEDAM)*, pp. 287 –292.

[12] Jemli, M., Ben Azza, H., Boussak, M. & Gossa, M. [2009]. Sensorless indirect stator field orientation speed control for single-phase induction motor drive, *IEEE Transactions on Power Electronics* 24(6): 1618–1627.

[13] Koubaa, Y. [2004]. Recursive identification of induction motor parameter, *Simulation Modelling Practice and Theory* 12(5): 368–381.
[14] Krause, P. C., Wasynczuk, O. & Sudhoff, S. D. [2002]. *Analysis of Electric Machinery and Drive Systems*, 2 edn, Wiley-IEEE Press.
[15] Lascu, C., Boldea, I. & Blaabjerg, F. [2005]. Comparative study of adaptive and inherently sensorless observers for variable-speed induction-motor drives, *IEEE Transactions on Industrial Electronics* 53(1): 57 – 65.
[16] Middleton, R. H. & Goodwin, G. C. [1990]. *Digital Control and Estimation - A Unified Approach*, 1 edn, Prentice Hall.
[17] Myers, M., Bodson, M. & Khan, F. [2011]. Determination of the parameters of non-symmetric induction machines, *Annual IEEE Applied Power Electronics Conference and Exposition (APEC)*, pp. 1028 –1033.
[18] Nied, A., de Oliveira, J., de Farias Campos, R., Jr., S. I. S. & de Souza Marques, L. C. [2011]. *Space Vector PWM-DTC Strategy for Single-Phase Induction Motor Control, Electric Machines and Drives, Miroslav Chomat (Ed.)*, InTech.
[19] Orlowska-Kowalska, T. & Dybkowski, M. [2010]. Stator-current-based mras estimator for a wide range speed-sensorless induction-motor drive, *IEEE Transactions on Industrial Electronics* 57(4): 1296 –1308.
[20] Rao, S., Buss, M. & Utkin, V. [2009]. Simultaneous state and parameter estimation in induction motors using first- and second-order sliding modes, *IEEE Transactions on Industrial Electronics* 56(9): 3369 –3376.
[21] Ribeiro, L. A. S., Jacobina, C. B. & Lima, A. M. N. [1995]. Dynamic estimation of the induction machine parameters and speed, *26th Annual IEEE Power Electronics Specialists Conference, PESC '95.* 2: 1281–1287 vol.2.
[22] Toliyat, H., Levi, E. & Raina, M. [2003]. A review of RFO induction motor parameter estimation techniques, *IEEE transactions on Energy conversion* 18(2): 271–283.
[23] Utkin, V. [1993]. Sliding mode control design principles and applications to electric drives, *IEEE Transactions on Industrial Electronics* 40(1): 23 –36.
[24] Vaez-Zadeh, S. & Reicy, S. [2005]. Sensorless vector control of single-phase induction motor drives, *Proceedings of the Eighth International Conference on Electrical Machines and Systems, 2005. ICEMS 2005* 3: 1838–1842 Vol. 3.
[25] van der Merwe, C. & van der Merwe, F. [1995]. A study of methods to measure the parameters of single-phase induction motors, *IEEE Transactions on Energy Conversion* 10(2): 248 –253.
[26] Vas, P. [1998]. *Sensorless Vector and Direct Torque Control*, Oxford Univ. Press.
[27] Velez-Reyes, M., Minami, K. & Verghese, G. [1989]. Recursive speed and parameter estimation for induction machines, *Conference Record of the Industry Applications Society Annual Meeting, 1989.* pp. 607–611 vol.1.
[28] Vieira, R. P., Azzolin, R. Z., Gastaldini, C. C. & Gründling, H. [2010]. Electrical parameters identification of hermetic refrigeration compressors with single-phase induction machines using RLS algorithm, *International Conference on Electrical Machines, 2010. ICEM 2010.*
[29] Vieira, R. P., Azzolin, R. Z. & Gründling, H. A. [2009]. A sensorless single-phase induction motor drive with a MRAC controller, *35st Annual Conference of IEEE Industrial Electronics Society, 2009.*, pp. 1003 –1008.
[30] Vieira, R. P., Azzolin, R. Z. & Gründling, H. A. [2009]. Parameter identification of a single-phase induction motor using RLS algorithm, *Brazilian Power Electronics Conference, 2009. COBEP '09.*, pp. 517 –523.
[31] Zahedi, B. & Vaez-Zadeh, S. [2009]. Efficiency optimization control of single-phase induction motor drives, *IEEE Transactions on Power Electronics* 24(4): 1062 –1070.